Barotropic Effects on Atmospheric Storm Tracks

SUKYOUNG LEE

Department of Meteorology, The Pennsylvania State University, University Park, Pennsylvania

(Manuscript received 4 September 1998, in final form 6 July 1999)

ABSTRACT

The effect of barotropic dynamics on atmospheric midlatitude storm tracks is investigated for the Northern Hemisphere winter season, using both observed data analyses and linear barotropic model experiments. It is shown that when the model flow is initialized with a realistic wave packet, barotropic processes alone can produce key features of the observed storm track structure. The author attributes this result both to the barotropic waveguide effect and to the fact that the geographical locations of barotropic growth coincide reasonably well with the baroclinic growth of the atmospheric storm track eddies.

This study also shows that barotropic dynamics are more relevant for storm tracks in lower latitudes than for those in higher latitudes, consistent with the fact that the lower-latitude storm tracks are more closely associated with the subtropical jet, rather than with the polar front jet that is driven by baroclinic eddies.

1. Introduction

Since the observed midlatitude storm tracks were described by Blackmon et al. (1977), storm tracks have been studied extensively (e.g., Frederiksen 1983a; Pierrehumbert 1984; Hoskins and Valdes 1990, among others). Although there is little doubt that baroclinicity of the atmosphere is vital for the existence of midlatitude storm tracks, recent studies have shown that barotropic dynamics can also play an important role for both the horizontal structure and the amplitude of the storm tracks (Branstator 1995; Lee 1995a; Whitaker and Dole 1995; Lee and Anderson 1996; Swanson et al. 1997). In particular, the barotropic model studies of Lee (1995a) and Swanson et al. (1997) take the perspective that absolute baroclinic instability (see Pierrehumbert 1984) is unlikely to be relevant for the atmospheric storm tracks (Lin and Pierrehumbert 1993; Lee 1995b), implying that the storm track eddies are continuously seeded by upstream disturbances. If this is indeed a correct picture, an upper-tropospheric waveguide must play an important role for the structure of the atmospheric storm track, as suggested by Lee and Anderson (1996).

Lee (1995a) and Swanson et al. (1997), using highly idealized barotropic models, have shown that ''barotropic modulation'' of waves by a zonally varying background flow can result in zonally localized storm tracks, when the storm track amplitude is defined in terms of nonconservative quantities, such as streamfunction variance and eddy kinetic energy. However, in these idealized models, the structure of the background flow is designed so that the wave energy is lost reversibly in the diffluent region downstream of the jet maximum, which then allows a secondary storm track of substantial amplitude to form after waves pass through the confluent region farther downstream. Specifically, a linear f-plane model was used by Lee (1995a), and a contour dynamics model by Swanson et al. (1997), for which meridional dispersion of Rossby waves is prohibited. Thus, in the latter study, unless wave breaking occurs due to nonlinear effects, wave energy cannot be lost irreversibly. Given these idealizations, it remains to be tested to what extent barotropic modulation is relevant for the atmospheric storm tracks.

While the above two studies focus on the changes in wave amplitude, Branstator (1995) and Lee and Anderson (1996) showed the possibility that the horizontal structure of the storm tracks is by and large determined by barotropic steering of the eddies by the background flow. However, these two studies differ from each other in that Branstator (1995) used a linearized version of the Community Climate Model to address the role of barotropic steering by background flows in the formation of storm track *anomalies*, whereas Lee and Anderson (1996) used a forced nonlinear barotropic model to address the role of barotropic dynamics in the formation of the *storm track itself*, rather than the anomalies. By examining the refractive index for the time mean flow of the nonlinear barotropic model, Lee and Anderson (1996) concluded that when the flow is re-

Corresponding author address: Dr. Sukyoung Lee, Department of Meteorology, The Pennsylvania State University, 503 Walker Bldg., University Park, PA 16802.
E-mail: sl@essc.psu.edu

laxed toward the observed time mean circulation of the Northern Hemisphere (NH) winter, a barotropic waveguide plays an important role for the horizontal structure of the storm track. Although it is interesting that this forced nonlinear barotropic model can simulate the structure of the atmospheric storm track to a reasonable degree, such a model has limitations for testing the conjecture that a barotropic waveguide is important for the formation of the atmospheric storm track. This is in part because the time mean flow of the barotropic model is not the same as the observed climatological flow, and because the eddies in the model exhibit somewhat different spectral characteristics (zonal wavenumber-frequency power spectra) than those observed in the atmosphere.

Given some of the shortcomings of the studies described above, this paper extends the above studies by addressing to what extent both the barotropic modulation of the wave amplitude and the barotropic waveguide can explain the structure of the *observed* NH winter storm track. This paper is organized as follows: Section 2 presents the data analysis that includes the 300-mb climatological flow, storm track, horizontal structure of the synoptic-scale waves, and refractive index of the synoptic-scale waves for the climatological flow. Section 3 describes results from a linear barotropic model that employs the climatological flow and the linearly regressed synoptic-scale waves as the background flow and initial perturbation, respectively. The concluding remarks follow in section 4.

2. Observations

In this study, daily National Centers for Environmental Prediction–National Center for Atmospheric Research reanalysis data is used, where the original data are converted to a rhomboidal spectral truncation at wavenumber 30. The climatological flow and eddy statistics for the NH winter are obtained from the 300-mb winds for December, January, and February (DJF), covering the time period of 1979–95. In this study, the synoptic-scale eddy statistics are obtained from 6-day high-pass filtered data.

Figure 1a shows the 300-mb high-pass streamfunction variance. As shown in previous studies (e.g., Blackmon et al. 1977), two local storm track maxima appear over the Pacific and Atlantic Oceans, known as the Pacific and Atlantic storm tracks, respectively. Upstream of the Pacific storm track, between 60° and 120°E, there are two additional storm track branches, one along 60°N, and the other along 30°N, as can be distinguished with the light shading. Throughout this paper, we refer to these storm track branches as the northern and southern branches, respectively. Note that for reference, the 300-mb climatological absolute vorticity (AV, hereafter) field is superimposed on all figures throughout this study, because the meridional gradient of the AV is a key quantity in the refractive index, upon which the wave guide idea is based. The properties of the refractive index indicate that a plane parallel, meridionally propagating wave bends toward a region of large meridional AV gradient. It can be seen that the southern branch is collocated with a region of strong meridional AV gradient that is associated with the subtropical jet. This correspondence, along with the fact that the 850-mb poleward eddy heat flux is essentially zero in this region (see Blackmon et al. 1977), suggests that the role of barotropic dynamics, that is, the waveguide effect and the amplification of eddies through barotropic processes, may be more prominent in this region.

As demonstrated with idealized models (Lee 1995a; Swanson et al. 1997), the degree of separation between the two oceanic storm tracks varies with the particular quantity used to measure the storm track. Figure 1b shows the 300-mb high-pass eddy kinetic energy (EKE). For an objective comparison between Figs. 1a and 1b, values greater than or equal to 65% of the maximum in each field are indicated by dark shading. By comparing the distance between the Pacific and Atlantic storm tracks, defined by the dark shaded area in both Figs. 1a and 1b, it is clear that the separation between the two oceanic storm tracks measured by the EKE is much less pronounced than that measured by the eddy streamfunction variance. This is consistent with the scaling arguments given by Lee (1995a) that the streamfunction variance should scale as the mean zonal wind to the fourth power while EKE should scale as mean zonal wind squared. This scale analysis indicates that as the wave packet moves into a region of weaker background zonal flow, the decrease in EKE should be smaller than that for the eddy streamfunction variance. Such a barotropic modulation of eddies occurs through a barotropic energy conversion between the eddies and background flow due to the horizontal variation of the structure of both the eddies and the background flow. Therefore, it is of interest to examine the structure of the barotropic energy conversion between the climatological background flow and the storm track eddies.

Figure 1c shows the barotropic energy conversion from the December–January–February (DJF) climatological flow to the synoptic-scale eddies. Throughout this paper, a positive (negative) barotropic energy conversion indicates that eddies gain (lose) energy from (to) the mean flow. In agreement with the barotropic energy conversions obtained by Wallace and Lau (1985) and Dole (1993), Fig. 1c shows three regions where eddies gain energy from the mean flow: east Asia and the western Pacific, North America, and North Africa and the Middle East. It is noteworthy that the former two regions are immediately upstream of the Pacific and Atlantic storm tracks, respectively. As alluded to by Dole (1993), these geographical relationships between the positive barotropic energy conversions and the two oceanic storm tracks suggest that positive barotropic energy conversions contribute toward the amplification of eddies in these two major storm tracks. It is also

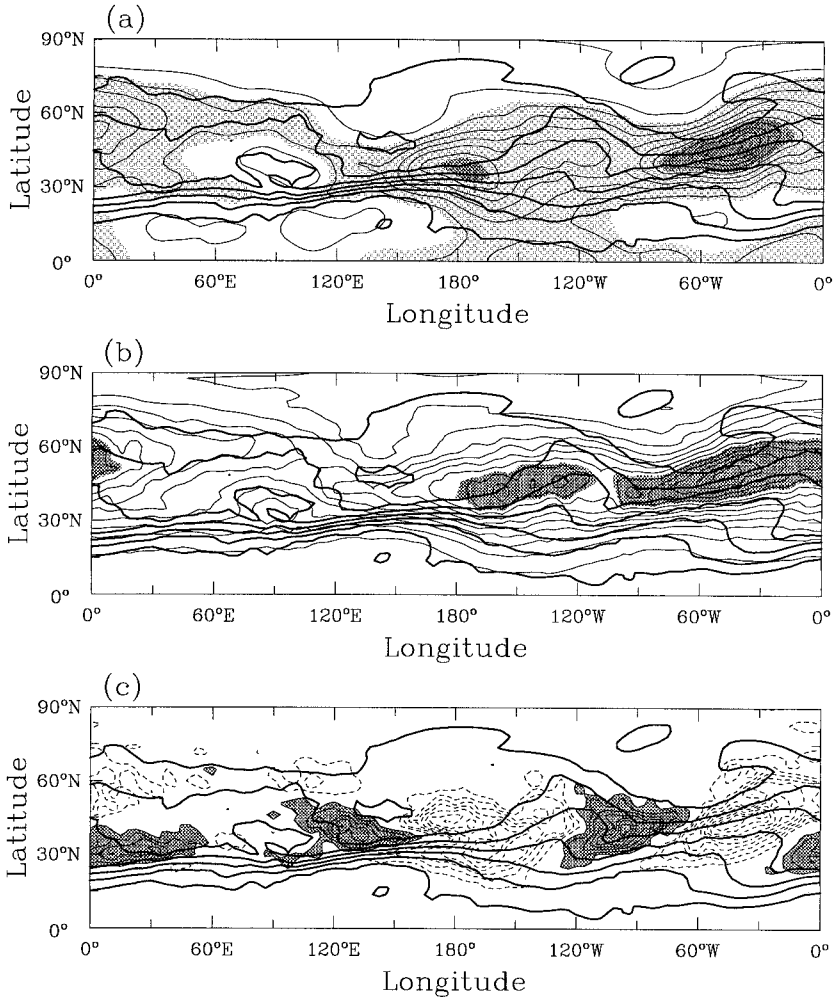

FIG. 1. The 300-mb DJF climatological high-pass (a) eddy streamfunction variance, (b) eddy kinetic energy, and (c) $-\overline{u'v'}(\partial\overline{u}/\partial y + \partial\overline{v}/\partial x) - \overline{u'^2}\partial\overline{u}/\partial y - \overline{v'^2}\partial\overline{v}/\partial x$ (barotropic energy conversion from the time mean flow to the transients). The contour interval is (a) 3×10^{12} m^4 s^{-2}, (b) 4 m^2 s^{-2}, and (c) 4×10^{-5} m^2 s^{-3}. Dark shaded areas represent values greater than or equal to 65% of the maximum for (a) and (b), and values greater than or equal to 4×10^{-5} m^2 s^{-3} for (c). Light shaded areas in (a) represent values greater than or equal to 8×10^{12} m^4 s^{-2}, but less than 65% of the maximum. Solid contours are positive, dashed contours negative, and the zero contour is omitted. The thick contours in (a)–(c) are the climatological absolute vorticity with a contour interval of 2×10^{-5} s^{-1}.

interesting to note that the southern branch lies immediately downstream of North Africa and the Middle East, which is one of the three regions where barotropic energy conversions are positive (see Figure 1c).

a. Regression analysis

In order to gain further insight into wave propagation in the storm track regions, and also for comparison with the results of the barotropic model experiments to be described later, it is useful to examine the structure of the observed synoptic-scale eddies. For this purpose, we calculate the time lagged high-pass streamfunction that is linearly regressed against the high-pass streamfunction at particular base points. In the regression equation, the amplitude of the eddy streamfunction at the base point is always set to one standard deviation. If the vorticity is regressed instead of the streamfunction, and an inverse Laplacian is applied to the regressed vorticity field, the results (not shown) are qualitatively very similar to those for the regressed streamfunction field.

Figures 2a–e show the regressed streamfunction field from lag -4 days to lag $+4$ days with the base point located at the center of the Pacific storm track (180° and 39.1°N). At lag -4 days, eddies in the upstream part of the wave packet are tilted northeast–southwest and mostly reside in the northern branch. Although eddies

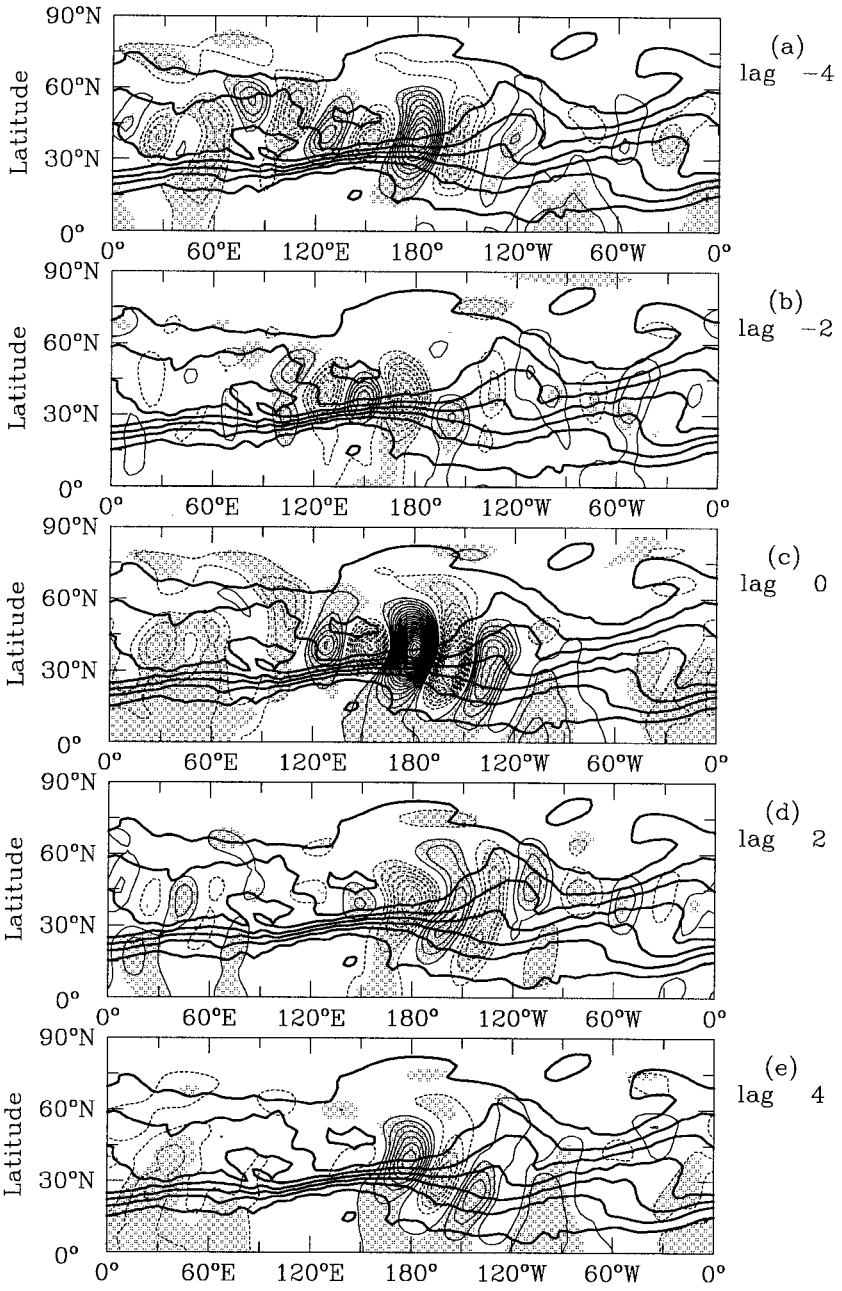

FIG. 2. Linear regression of the band-pass streamfunction field with base point at 39.1°N, 180° for (a) lag −4, (b) lag −2, (c) lag 0, (d) lag +2, and (e) lag +4 days. Contour interval is 2×10^5 m^2 s^{-1} and the zero contour is omitted. The shaded area represents regions where statistical significance exceeds the 95% confidence level. The thick contours in (a)–(e) are the climatological absolute vorticity with a contour interval of 2×10^{-5} s^{-1}.

are present in the southern branch from lag −4 days to lag 0, the amplitude of these eddies is much smaller than those in the northern branch. Thus, it appears that the main source of disturbances for the Pacific storm track comes from the northern branch.

As the eddies continue to propagate into the region of weak absolute vorticity (AV) gradient, between 180° and 90°W, they are stretched meridionally, sometimes breaking into two (see Fig. 2d), one to the north, and the other to the south. Figures 2c–e suggest that it is the eddies to the north that propagate into the Atlantic storm track region. The same conclusion can be drawn from Figs. 3a, 3b, and 3c, which show the regressed streamfunction fields at lags −4, −2, and 0 days, respectively, with the base point located at 45.8°N and 45°W, the center of the Atlantic storm track. The re-

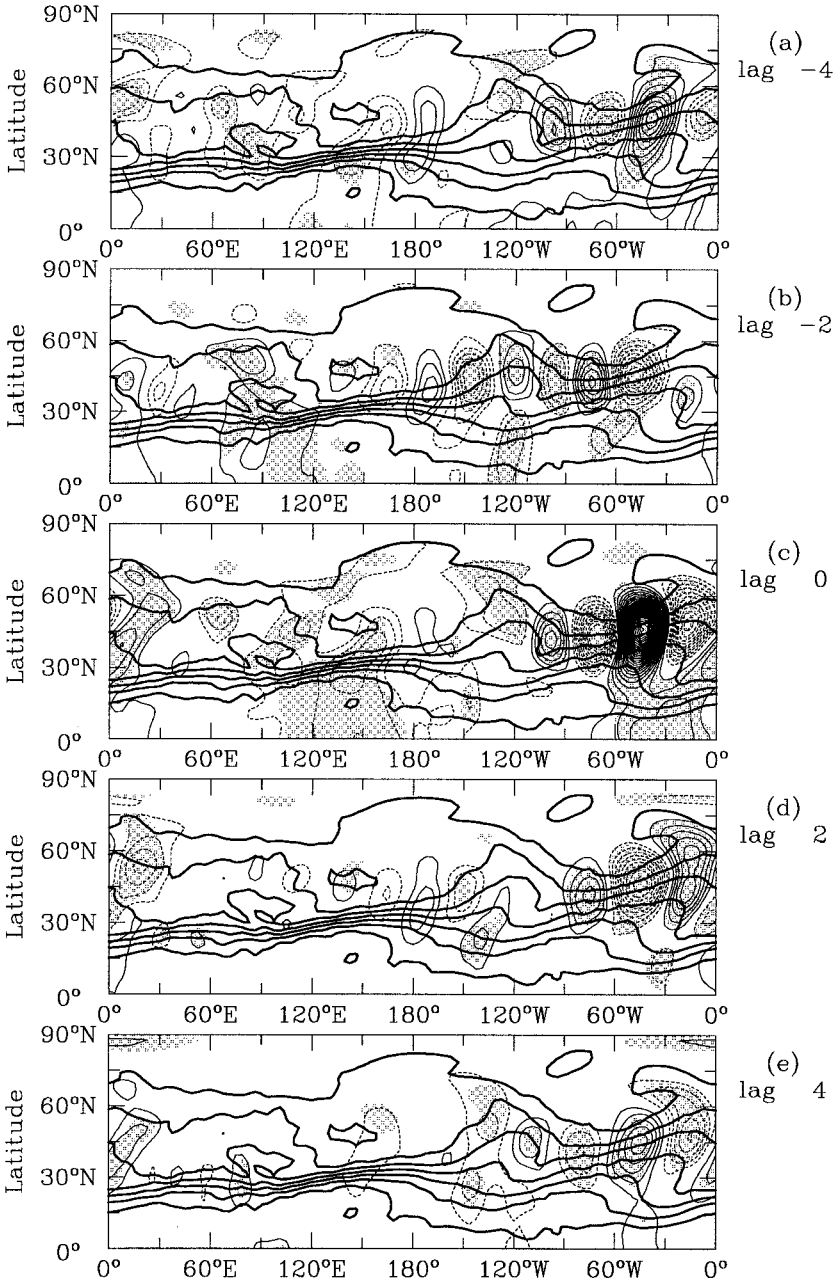

FIG. 3. As for Fig. 2 except that the base point is at 45.8°N, 45°W.

gressed streamfunction field at lag 0 shows a prominent northeast–southwest tilt over the Greenwich meridian, indicating equatorward propagation of the Atlantic storm track eddies in this region. At lags +2 (Fig. 3d) and +4 days (Fig. 3e), one can see small-amplitude eddies along the southern branch, in particular, following the strong AV gradient. As indicated earlier, this AV gradient is associated with the subtropical jet. Because equatorward propagating eddies gain energy from the basic flow in the cyclonic shear zone, one expects a positive barotropic energy conversion on the poleward side of the strong AV gradient, as shown in Fig. 1c.

b. Refractive index

In order to investigate if the structure of the atmospheric storm track eddies are consistent with the upper-tropospheric waveguide, we examine the refractive index, *n*, whose description can be found in Lee and Anderson (1996). The refractive index is a function of the

meridional potential vorticity gradient, the zonal wind speed of the background flow, and the zonal wavenumber and frequency of the wave. Within the context of linear theory, if waves with the appropriate structure and frequency are present within the waveguide, these waves can propagate. On the other hand, in the region where n is imaginary, waves are evanescent.

Unlike the nonlinear barotropic model of Lee and Anderson (1996), where the model's synoptic-scale eddies have a single, distinctive value for their zonal wavenumber throughout the midlatitudes, for the observations, the dominant zonal wavenumber varies between different storm tracks. From the regressed eddy fields, we estimate that the dominant zonal wavenumber is 8 and 7 over the southern branch and the Pacific storm track, respectively, and that zonal wavenumber 6 is dominant over both the Atlantic storm track and the northern branch. The typical period for these waves, again estimated from the lagged regression fields, is 4 days for each storm track. Figures 4a, 4b, 4c, and 4d show $\mathrm{sgn}(n^2)|n|$, for $\omega = 2\pi/4$ day^{-1} and $m = 8$, 7, 6, and 6, respectively. The propagating region is indicated by shading. For direct comparison between the refractive index and the synoptic-scale eddies along each storm track, lag-0 regressed eddy fields are superimposed on each frame in Fig. 4.

The agreement between the location of the storm track eddies and the propagating region (i.e., real n) is good for the southern branch (Fig. 4a), in particular between 60° and 150°E. For the Pacific storm track, the agreement is rather poor in the upstream half; however, it is reasonable in the downstream half. For both the Atlantic storm track and the northern branch, the agreement is reasonably good.

3. Linear barotropic model experiments

On the premise that barotropic dynamics is relevant for midlatitude storm tracks to the extent that it modulates the amplitude of the baroclinic eddies and steers the baroclinic eddies to yield their geographical distribution, linear barotropic model experiments are performed. This approach takes the viewpoint that the eddy evolution in this barotropic initial value calculation can be thought of as being representative behavior of the temporal evolution of storm track eddies. With this perspective, we will attempt to compare the results from the linear barotropic model with the climatological storm track in the atmosphere. For the model experiments, we specify the background flow as the observed 300-mb DJF climatological flow and the initial perturbation as a realistic midlatitude disturbance. We limit the length of the model integrations for a period less than or equal to 15 days, for the following two reasons. First, when the linear barotropic model is integrated for a sufficiently long time, an unstable normal mode emerges that is similar to the most unstable normal mode described by Frederiksen (1983b) and Simmons et al. (1983). Because such an unstable mode is not the subject of this study, it is desirable to stop the integration before such an unstable mode emerges. Second, since the goal of the model experiment is to examine the storm track structure some distance downstream of the initial wave packet, not the storm track for the entire model atmosphere, it is not necessary to extend the integration beyond the time the packet takes to traverse one latitude circle.

We note that nonlinear barotropic model integrations were also performed. The results are not shown because, for the limited time integration, they are very similar to the results of the linear model experiments.

Specifically, we attempt to address the following question: if one starts with a realistic synoptic-scale disturbance, to what degree can the observed storm track be reproduced with barotropic dynamics alone? The weakness of this approach is that it does not address how the realistic synoptic-scale eddies are initially generated. Without a doubt, baroclinic effects must be playing a central role in determining the amplitude of the eddies. On the other hand, the strength of this approach is that it allows one to address barotropic effects on storm tracks in a more controlled setting.

This model is governed by the linearized barotropic vorticity equation:

$$\frac{\partial \zeta'}{\partial t} = -J(\overline{\psi}, \zeta') - J(\psi', f + \overline{\zeta}) - \nu\nabla^8\zeta'. \quad (1)$$

The notation is standard, and ν is the quad-harmonic diffusion coefficient with a value of 8×10^{37} m^8 s^{-1}. Such highly scale selective diffusion is chosen to minimize dissipation on the energy containing eddies. The overbar denotes the DJF climatological flow at 300 mb, and the prime the deviation from this state. The model resolution is truncated at rhomboidal 30 (R30).

In order for the results from this initial value problem to be compared with the observed time mean storm track, it is desirable to select an initial wave packet that is representative of the observed storm track eddies. For this reason, we use the regressed lag 0 synoptic-scale eddies as the initial disturbance (see Figs. 2c and 3c). In order to focus on the wave packet evolution, the regressed eddy field is multiplied by a weighting function so that the amplitude of the regressed field slowly decays to zero away from the wave packet. This weighting function takes the form of

$$w(i, j) = \begin{cases} [\cos(\pi(i - i_0)/2L_x)\cos(\pi(j - j_0)/2L_y)]^{1/2} \\ \quad \text{if } |i - i_0| \le L_x \text{ and } |j - j_0| \le L_y \\ 0 \quad \text{otherwise,} \end{cases}$$

where i and j refer to longitude and latitude points on the Gaussian grid, and $L_x = 20$ and $L_y = 10$, corresponding to 75° longitude and 22.3° latitude, respectively. Note that with a R30 truncation, there are 96 and 80 grid points in the zonal and meridional directions, respectively. The point (i_0, j_0) corresponds to the base point of the linear regression. Once this new field is

obtained, the global mean of this initial vorticity field is set equal to zero. It should be noted that except at the base point, the amplitude of the regressed lag 0 synoptic-scale eddies is only a fraction of the climatological storm track amplitude. Therefore, when comparing the storm track amplitude of the barotropic model with that of observations, one should measure the relative amplitude of the model (e.g., the amplitude of the Atlantic storm track relative to that of the Pacific storm track) rather than the absolute amplitude.

a. Initial wave packet at the Pacific storm track

Figures 5a–e show the temporal evolution of a wave packet placed initially at 180° and 39.1°N, where the streamfunction amplitude is greatest within the Pacific storm track. Note that although in principle a different wave phase can be chosen within the wave packet, in practice the phase is not the subject of an arbitrary choice. This is because the wave packet is obtained from the regression analysis and, as stated above, the geographical location of the base point is chosen so that it corresponds to the point of the maximum streamfunction amplitude within the observed Pacific storm track.

In these figures, as for the observational analyses, the DJF climatological AV at 300 mb is superimposed as a reference field. The times for these snapshots are based on the temporal characteristics of the ⟨EKE⟩ field, where the phase averaging denoted by ⟨ ⟩ is determined in the following manner. The phase averaging is obtained by first calculating the dominant zonal wavenumber of the wave packet at each latitude, followed by the performance of a spatial running mean of the EKE over the zonal wavelength corresponding to the dominant zonal wavenumber. Such phase averaging is performed to quantify wave energy and energy conversion. A time series of the maximum value of the ⟨EKE⟩ field for the entire domain is then generated, and the times selected for Fig. 5 correspond to the time of the (a) first local ⟨EKE⟩ maximum, (b) first local ⟨EKE⟩ minimum, (c) second local ⟨EKE⟩ maximum, (d) second local ⟨EKE⟩ minimum, and (e) the third local ⟨EKE⟩ maximum. The temporal evolution of the corresponding ⟨EKE⟩ field is shown in Fig. 6.

Because the wave packet is sufficiently localized in space, we examine the changes in ⟨EKE⟩ of the wave packet in a reference frame that moves with the wave packet. Upon integrating the equation for ⟨EKE⟩ over both the entire domain and the time interval of interest, from t_1 to t_2, one obtains

$$\int_y \int_x \langle \mathrm{EKE}(t_2) \rangle - \langle \mathrm{EKE}(t_1) \rangle \, dx \, dy = -\int_y \int_x \int_{t_1}^{t_2} \left[\langle u'^2 \rangle \frac{\partial \overline{u}}{\partial x} + \langle v'^2 \rangle \frac{\partial \overline{v}}{\partial y} + \langle u'v' \rangle \left(\frac{\partial \overline{u}}{\partial y} + \frac{\partial \overline{v}}{\partial x} \right) \right] dt \, dx \, dy. \quad (2)$$

Figure 7a shows the energy conversion term [the integrand of the rhs of (2)] integrated from day 0 to day 2.4. Equation (2) states that the global integral of the quantity shown in Fig. 7a must be equal to the global integral of ⟨EKE⟩ at day 2.4 (Fig. 6b) minus that at day 0 (Fig. 6a). A calculation of these quantities yields a difference of 14%, which seems acceptable for the purpose of relating the change in ⟨EKE⟩ to the energy conversion, and also seems reasonable given the presence of subgrid-scale dissipation and the uncertainties involved in the phase average of eddy variances. As stated earlier, because both the wave packet and the energy conversion are spatially localized, we interpret the changes in ⟨EKE⟩ of the wave packet from day 0 (Fig. 6a) to day 2.4 (Fig. 6b) as being due to the energy conversion integrated from day 0 to day 2.4 (Fig. 7a). Similarly, we interpret the ⟨EKE⟩ changes from Fig. 6b to Fig. 6c, from Fig. 6c to Fig. 6d, and from Fig. 6d to Fig. 6e as being due to the barotropic energy conversion in Figs. 7b, 7c, and 7d, respectively.

At the time of the first local ⟨EKE⟩ minimum (Fig. 6b), the center of the wave packet lies in the region where the meridional AV gradient exhibits a local minimum, which coincides with a local minimum in the zonal wind. Consistent with the observations and also with the scaling arguments reviewed earlier, the wave packet in this region is meridionally elongated (see Fig. 5b), although the linear barotropic model exaggerates the NE–SW tilting south of ≈40°N. Figure 7a indicates that the decrease in ⟨EKE⟩ from day 0 to day 2.4 is, by and large, due to energy loss to the background flow in the diffluent region, between 170°E and 120°W. North of ≈40°N, where the horizontal tilt of the eddies is small, the meridional stretching is followed by shrinking as the wave packet propagates into the region of stronger zonal winds (Fig. 5c), resulting in the secondary ⟨EKE⟩ maximum (Fig. 6c). Again, this is consistent with the net energy gain from the background flow in the confluent region during this time period (see Fig. 7b). East of 70°W, the waves are unable to further amplify, because the background flow becomes diffluent toward the central region of the observed Atlantic storm track. In addition, the meridional dispersion of eddies reduces the eddy amplitude in this region, disabling the linear barotropic model from depicting the main body of the Atlantic storm track. Although such meridional dispersion also exists in the atmosphere in that region (see Fig. 2c), compared with the observations, the northeast–

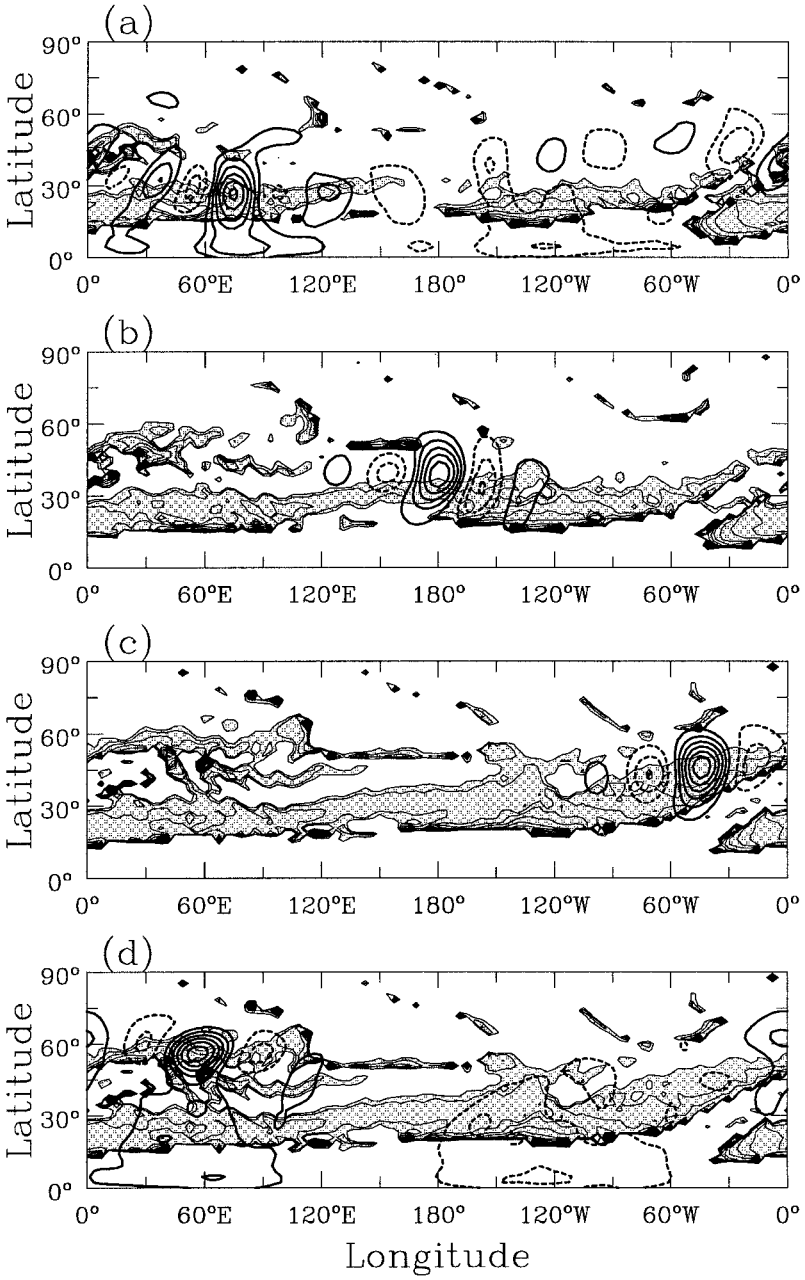

FIG. 4. The thin contours are for the refractive index, $\mathrm{sgn}(n^2)|n|$ for $T = 4$ days and (a) $k = 8$, (b) $k = 7$, (c) and (d) $k = 6$. Only positive values are contoured, and the contour interval is 4. Shading indicates positive values of $\mathrm{sgn}(n^2)|n|$. The thick contours are for the linear regression of the band-pass streamfunction field at lag zero, with base point at (a) 25.7°N, 75°E, (b) 39.1°N, 180°, (c) 45.8°N, 45°W, and (d) 54.8°N, 56.25°E. The contour interval is 4×10^5 m^2 s^{-1} for (a) and (d), and 8×10^5 m^2 s^{-1} for (b) and (c). Solid contours are positive, dashed contours negative, and the zero contour is omitted.

southwest tilt of the eddies in the model is too strong. This result indicates that while barotropic modulation does play a role in the amplification of eddies in the Atlantic storm track, baroclinicity is essential in explaining the bulk of the Atlantic storm track, even when realistic synoptic-scale eddies are supplied from the Pacific storm track region. However, the barotropic effect on the baroclinic amplification of the storm track eddies may be more subtle than that described above. This is because the baroclinic growth that arises from pre-existing upper-level disturbances depends on the amplitude of the upper-level disturbances, and these upper-

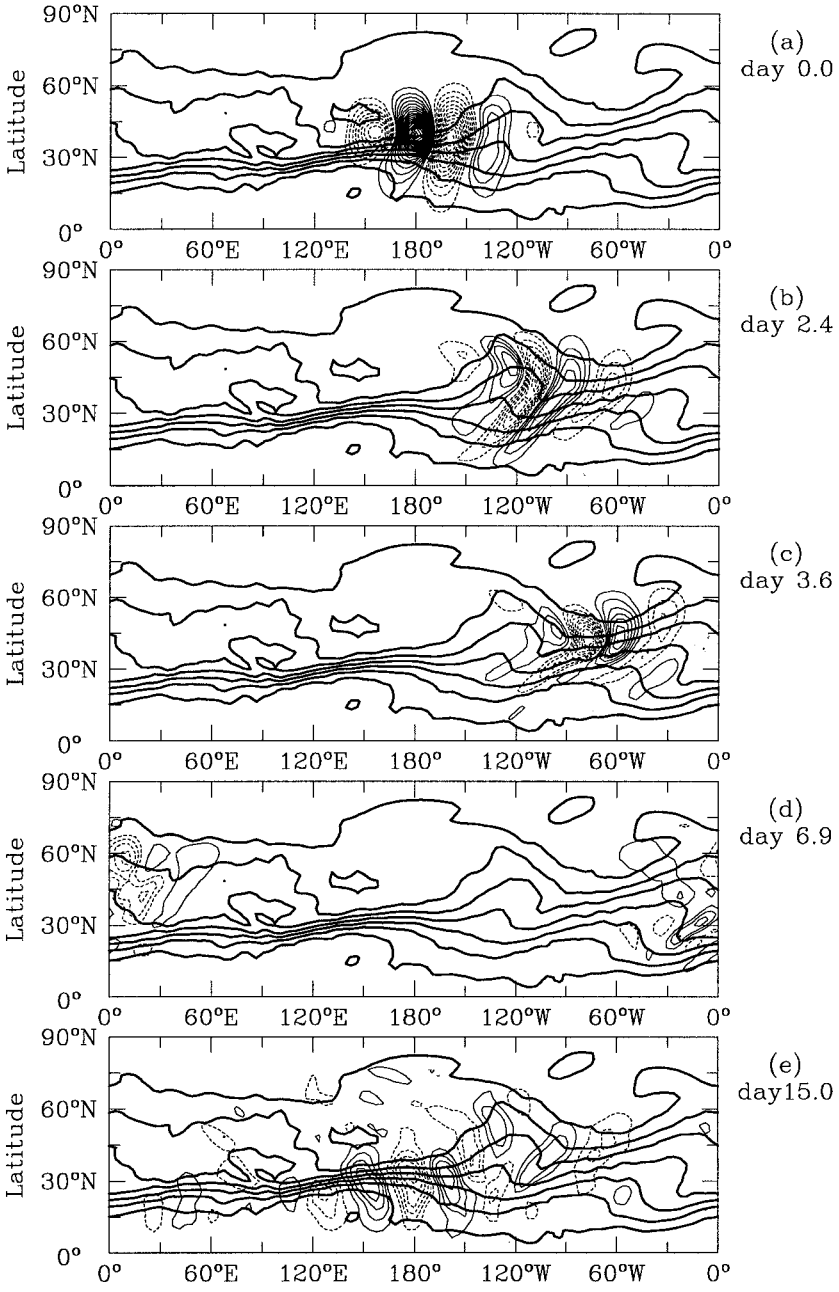

FIG. 5. The model streamfunction field at day (a) 0, (b) 2.4, (c) 3.6, (d) 6.9, and (e) 15, for an initial wave packet centered at 39.1°N and 180°. The contour interval is 1.5×10^5 m^2 s^{-1} and the zero contour is omitted. Solid (dashed) contours are for positive (negative) values. The climatological absolute vorticity field (thick contours) is superimposed on (a)–(e) with a contour interval of 2×10^{-5} s^{-1}.

level disturbances are, in part, amplified by the barotropic modulation at the upstream end of the Atlantic storm track.

Downstream of the Atlantic storm track, the wave packet splits into two; one part located along the northern branch and the other along the southern branch (see Figs. 5d and 6d), although the wave amplitude along the latter is very small. From Fig. 7c, we attribute the decrease in ⟨EKE⟩ in this region to the energy loss to the mean flow in the diffluent region between 60°W and the Greenwich meridian. The two wave packets then continue to propagate eastward along both the northern and southern branches, with that along the latter being more prominent as shown in Fig. 5e. By day 15, the two wave packets become a single wave packet centered at 180°, the same longitude where the initial wave packet

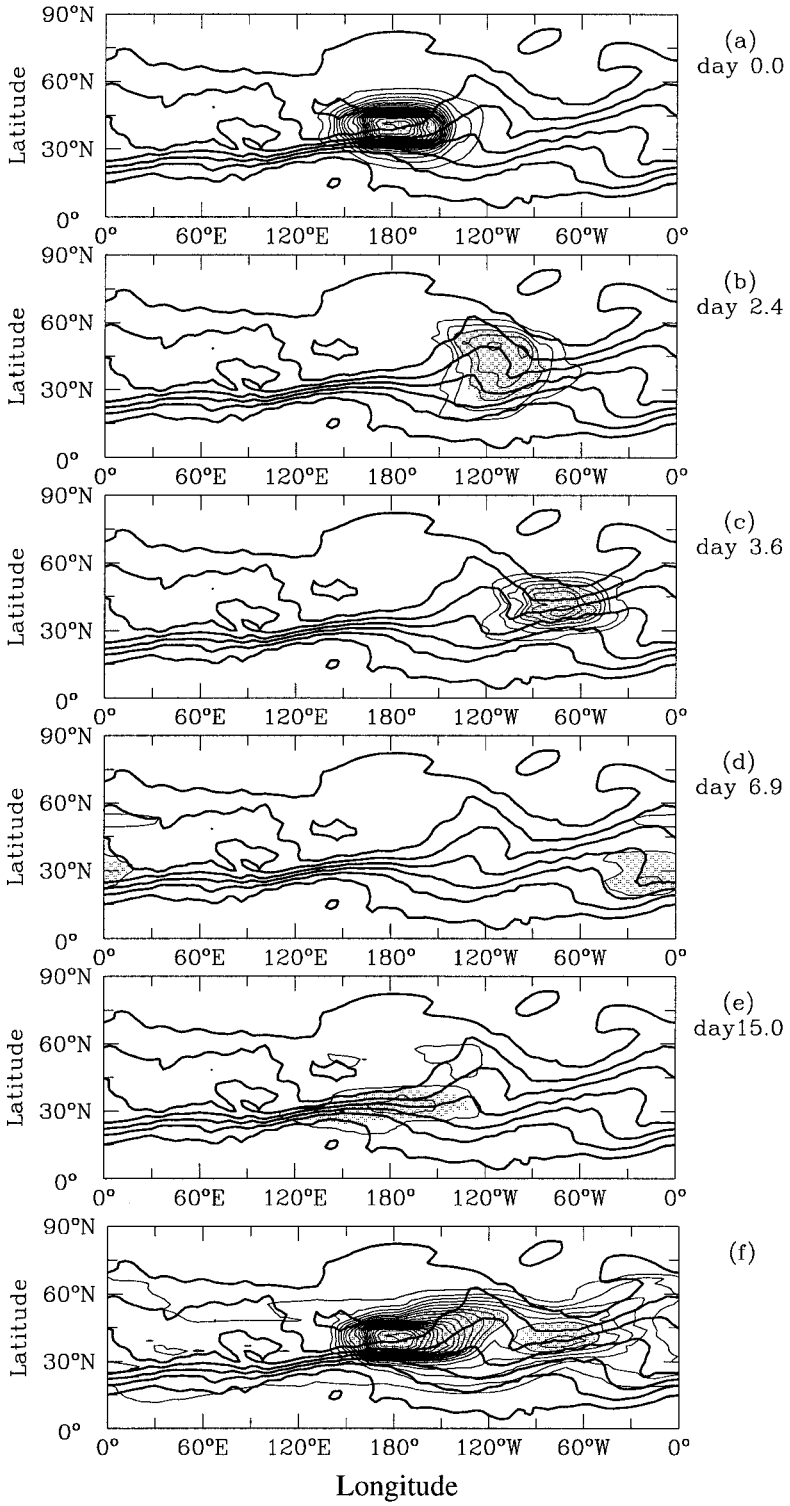

FIG. 6. The model phase-averaged EKE at day (a) 0, (b) 2.4, (c) 3.6, (d) 6.9, (e) 15, and (f) the maximum value of EKE at a each location during the 15-day period. The initial wave packet is centered at 39.1°N and 180°, and the contour interval is 0.2 $m^2 s^{-2}$. Shading denotes values greater than or equal to 30% of the maximum. The climatological absolute vorticity field (thick contours) is superimposed on (a)–(f) with a contour interval of $2 \times 10^{-5} s^{-1}$.

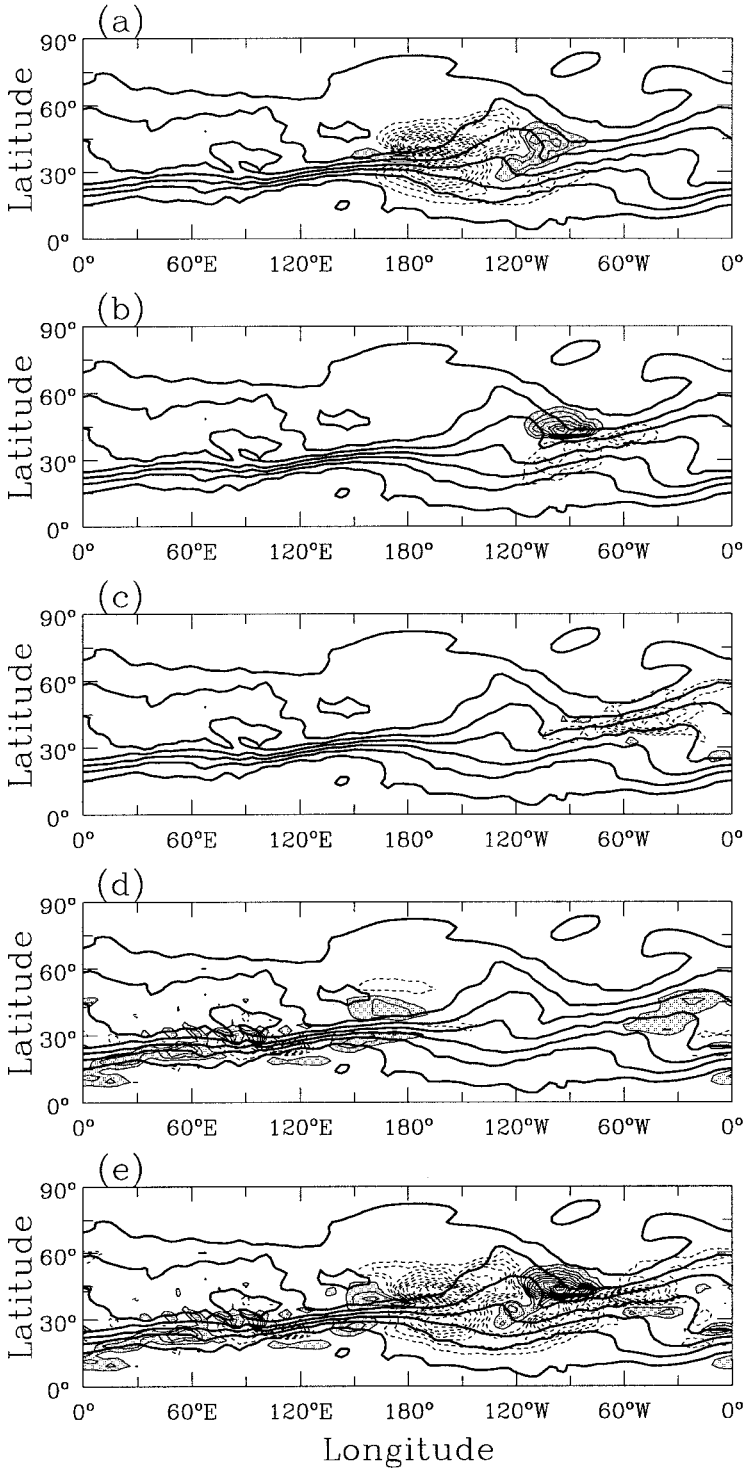

FIG. 7. The model phase-averaged barotropic energy conversion, integrated between days (a) 0 and 2.4, (b) 2.4 and 3.6, (c) 3.6 and 6.9, (d) 6.9 and 15, and (e) 0 and 15. The initial wave packet centered at 39.1°N and 180°. The contour interval is 0.2 m^2 s^{-2} and the zero contour is omitted. Solid (dashed) contours are for positive (negative) values. The climatological absolute vorticity field (thick contours) is superimposed on (a)–(e) with a contour interval of 2×10^{-5} s^{-1}.

was placed, although the latitudinal location and structure of the waves differ from those of the initial wave packet (compare Figs. 5a and 5e). Also, the maximum ⟨EKE⟩ amplitude at day 15 is greater than that at day 6.9, owing to the energy gain from the background flow, mostly along the southern branch (see Fig. 7d). Although a precise comparison between the model and observations is inappropriate, as the latter does not possess as well-defined a wave packet as in the model, such a positive barotropic energy conversion is also found along the southern branch in the observational data (see Fig. 1c). It is also interesting to note that such an unforced wave packet in a barotropic flow is able to propagate around a latitude circle with its structure reasonably intact.

The amplitude modulation of the wave packet is succinctly summarized by a horizontal map of $\langle \mathrm{EKE} \rangle_{\max}$, as shown in Fig. 6f, where $\langle \mathrm{EKE} \rangle_{\max}$ is the maximum ⟨EKE⟩ at each grid point during the 15 days of the model integration. This is because at a given point, $\langle \mathrm{EKE} \rangle_{\max}$ must occur when the center of the wave packet lies at that point. Figure 6f shows two distinctive ''storm tracks'' that exhibit a reasonable degree of resemblance to those in observations (see Fig. 1b), although the model's Atlantic storm track is much too weak. Figure 7e shows the energy conversion integrated from day 0 to day 15. In the Western Hemisphere, the structure of the barotropic energy conversion in the model reasonably resembles that in the observations.

Although not shown here, we performed additional numerical experiments to examine the sensitivity of the above results to the latitudinal location of the initial wave packet. For all of these experiments, the initial wave packets are obtained from the regressed lag 0 synoptic-scale eddies at corresponding latitudes. We found that the secondary maximum at the Atlantic storm track region appears when the initial wave packet is placed between 34.5° and 43.6°N. Note that these values correspond to the Gaussian latitudes at R30 truncation. Apparently, when the center of the initial wave packet lies outside of this latitude band, the structures of the synotic-scale waves and the background flow do not allow enough wave energy to be lost *reversibly*.

b. Initial wave packet at the Atlantic storm track

In order to more closely examine the role of barotropic dynamics in the Eastern Hemisphere, we perform a second experiment with the initial wave packet located at the center of the Atlantic storm track (see Fig. 8a). In this case, the results are presented for a 9.3-day model integration. As for the experiment described in section 3a, the eddy streamfunction, ⟨EKE⟩, and time integrated barotropic energy conversions are examined, and they are shown in Figs. 8, 9, and 10, respectively.

As for the observations (Figs. 3c–e), downstream of the Atlantic storm track, the eddies are elongated meridionally and show a pronounced northeast–southwest tilt (Fig. 8b) toward the southern branch. At the same time, the amplitude of the ⟨EKE⟩ decreases (Figs. 9a and 9b) due to the energy loss in the diffluent region (Fig. 10a). As the wave packet propagates farther eastward, amplification of ⟨EKE⟩ occurs in the southern branch (Fig. 9c). This is consistent with the positive barotropic energy conversion in the northern end of the southern branch (Fig. 10b). Such a structure in the energy conversion is also found in the observations (Fig. 1c), once again consistent with the fact that the eddies exhibit northeast–southwest tilt in this region (Fig. 4a) where the zonal wind decreases with latitude. Evidently, in the observations, the EKE of the northern branch is much greater than that of the southern branch because baroclinic processes are much more crucial in the former region.

Once the southeastward propagating wave packet reaches the southern branch, characterized by a strong meridional AV gradient, the southward propagation is halted (Fig. 8c), and the eddies rotate to exhibit a northwest–southeast structure (Fig. 8d). Such a change in the eddy structure can also be seen (Fig. 4a) and inferred (Fig. 1c) in the observations. As the wave packet propagates into the Pacific storm track region, there is a slight increase in the maximum ⟨EKE⟩ (cf. Figs. 9d and 9e). We attribute this amplification of ⟨EKE⟩ and eddy streamfunction mostly to the interaction between the southeastward propagating eddies from the northern branch and the cyclonic shear associated with the Pacific jet (see the positive conversion centered at 180° in Fig. 10d). Upstream of the Pacific storm track, a positive energy conversion can also be found in the observations (Fig. 1c), although the center lies at 135°E, rather than at 180°. As shown in Fig. 9f, such an amplification yields a local maximum in ⟨EKE⟩, in the region of the Pacific storm track, although its magnitude is much smaller than the observed Pacific storm track.

4. Concluding remarks

This paper examines the role of barotropic dynamics for atmospheric storm tracks using both observational analyses and linear barotropic model experiments. We conclude that the barotropic model's storm track structure captures some of the essential features of the atmospheric storm track, because the geographical location of the baroclinic and barotropic energy conversions in the atmosphere are reasonably close to each other, and because the structure of the model's barotropic energy conversion is similar to that for the atmosphere in the storm track regions. The latter agreement, in turn, owes to the fact that the geographical location and the structure of the model's eddies resemble those of the atmospheric storm track eddies to a reasonable degree. Because baroclinic processes are absent in the barotropic model, we attribute such a resemblance to an operation of the barotropic waveguide on storm track eddies in the upper troposphere. Calculation of the re-

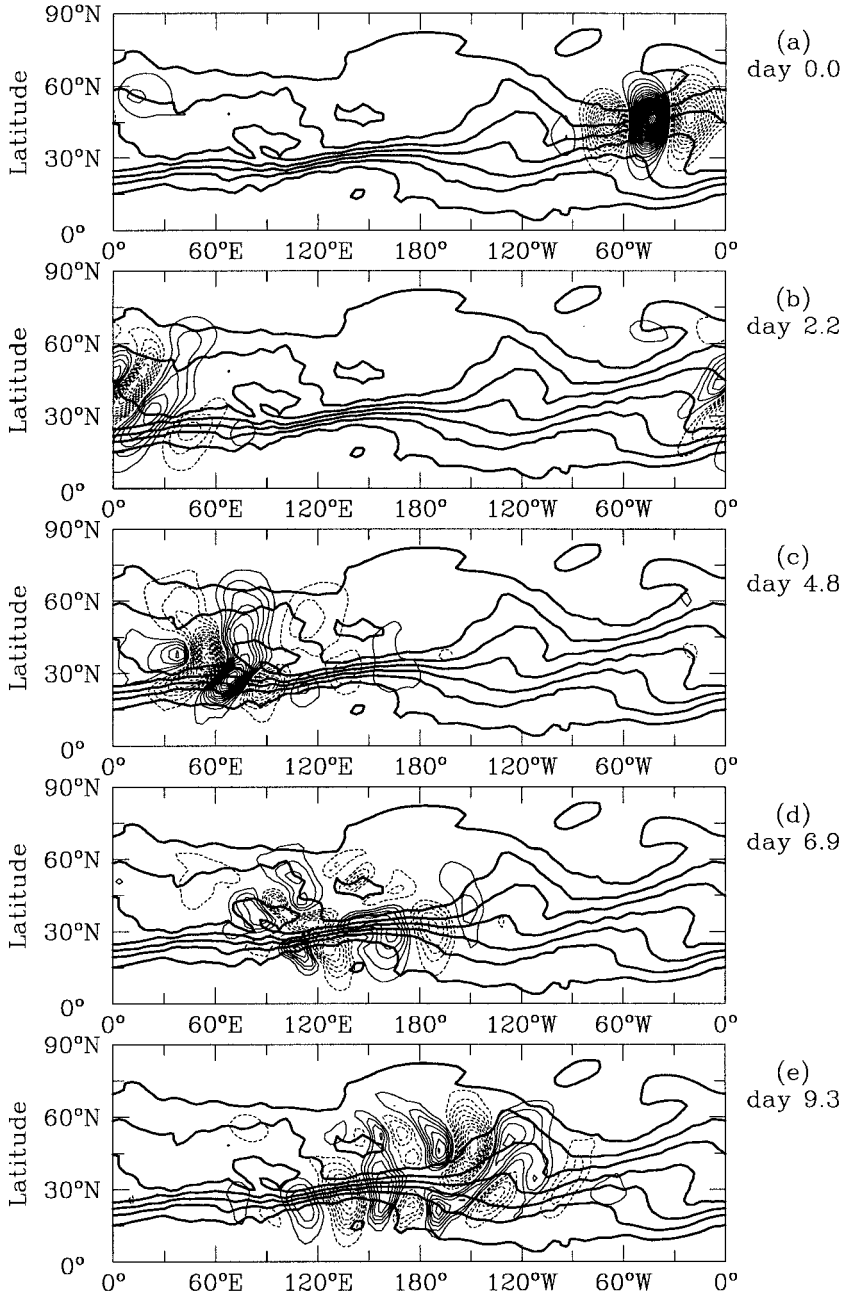

FIG. 8. The model streamfunction field at day (a) 0, (b) 2.2, (c) 4.8, (d) 6.9, and (e) 9.3, for an initial wave packet centered at 45.8°N and 45°W. The contour interval is 1.5×10^5 m^2 s^{-1} and the zero contour is omitted. Solid (dashed) contours are for positive (negative) values. The climatological absolute vorticity field (thick contours) is superimposed on (a)–(e), with a contour interval of 2×10^{-5} s^{-1}.

fractive index for the Rossby waves with the observed 300-mb climatological flow supports such a conjecture.

Although this study shows that for a limited amount of time (10–15 days) barotropic process alone can produce some of the observed storm track structure, it still remains to be determined to what degree the barotropic processes are important for the observed storm track structure. Such a degree might be measured by the ratio of the amplitude of the secondary storm track (e.g., Atlantic storm track when the wave packet is initialized at the Pacific storm track, and vice versa) in the barotropic model to its counterpart in the observations. In that case, it is found that the degree to which the barotropic processes contribute to the storm track amplitude

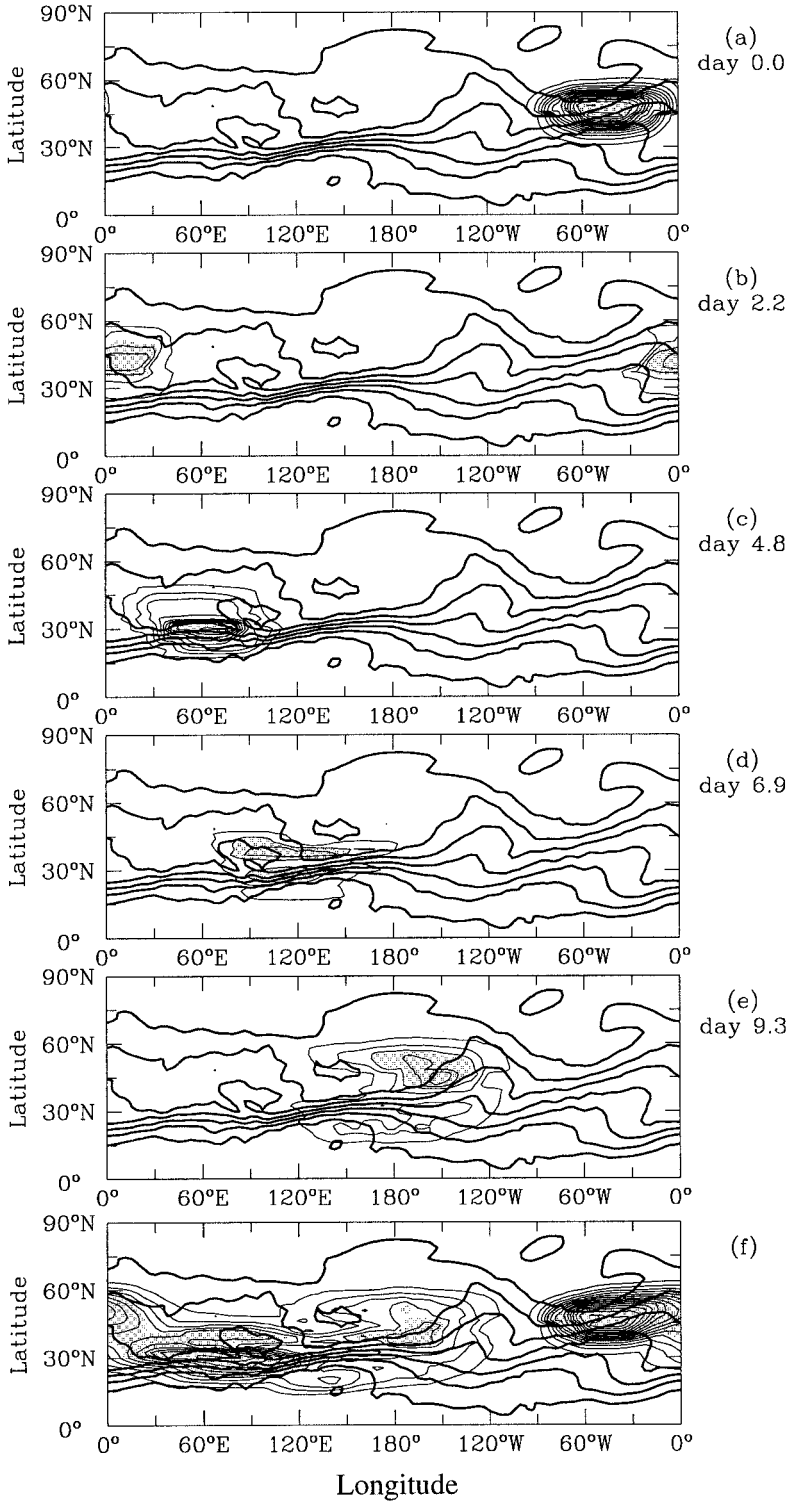

FIG. 9. The model phase-averaged EKE at day (a) 0, (b) 2.2, (c) 4.8, (d) 6.9, (e) 9.3, and (f) the maximum value of EKE at each location during the 15-day period. The initial wave packet is centered at 45.8°N and 45°W, and the contour interval is 0.4 $m^2 s^{-2}$. Shading denotes values greater than or equal to 30% of the maximum. The climatological absolute vorticity field (thick contours) is superimposed on (a)–(f) with a contour interval of 2×10^{-5} s^{-1}.

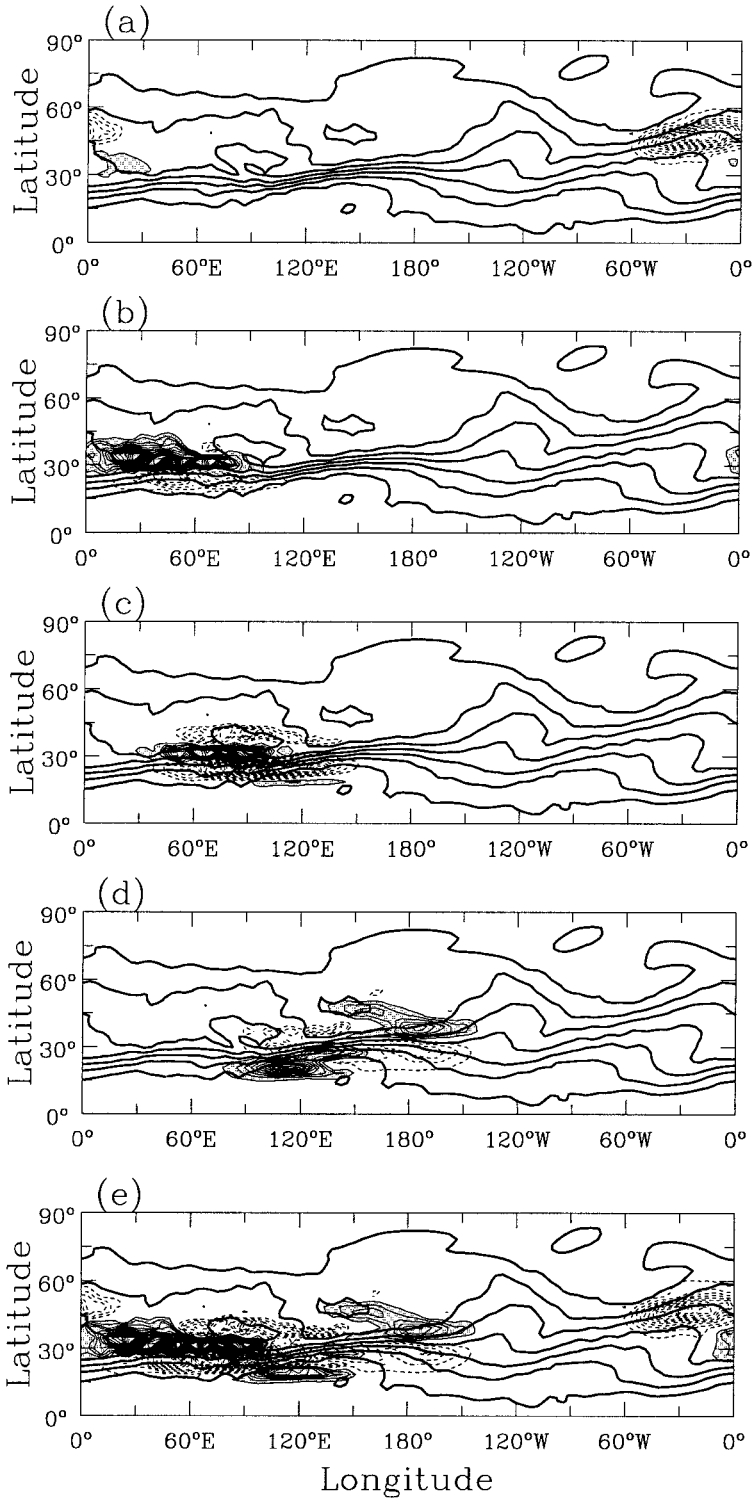

FIG. 10. The model phase-averaged barotropic energy conversion, integrated between days (a) 0 and 2.2, (b) 2.2 and 4.8, (c) 4.8 and 6.9, (d) 6.9 and 9.3, and (e) 0 and 9.3. The initial wave packet is centered at 45.8°N and 45°W. The contour interval is 0.4 $m^2\ s^{-2}$ and the zero contour is omitted. Solid (dashed) contours are for positive (negative) values. The climatological absolute vorticity field (thick contours) is superimposed on (a)–(e), with a contour interval of $2 \times 10^{-5}\ s^{-1}$.

is rather small according to the linear barotropic model experiment presented in this study. In other words, the secondary storm track in the linear barotropic model is much too weak to explain its counterpart in the atmosphere. However, this is because in the linear barotropic model, much of the wave energy is irreversibly lost in the diffluent region upstream of the secondary storm track. In the atmosphere, we expect that barotropic energy modulation is stronger than that implied in the linear barotropic model because of the continued wave amplification due to baroclinic processes. For a more quantitative assessment of the contribution by barotropic modulation toward the atmospheric storm track structure, a baroclinic source for the storm track eddies needs to be appropriately represented in the model experiments.

The experiments with the linear barotropic model also suggest that barotropic dynamics is more relevant for the storm tracks along North Africa and the Middle East than along Europe and Russia. In this study, the former is referred to as the southern branch and the latter as the northern branch. Barotropic dynamics are more relevant for the southern branch in part because the eddies that propagate equatorward from the Atlantic storm track gain energy from the mean flow as they encounter the cyclonic shear on the poleward side of the subtropical jet. Due to a large absolute vorticity gradient along the subtropical jet, once the eddies reach the subtropical jet, they propagate along the subtropical jet rather than continue to propagate toward the equator. The refractive index calculation shows that this behavior can be interpreted as a waveguide effect. However, considering the strong absolute vorticity gradient associated with the subtropical jet, it is also possible that the eddies are being ''trapped'' within the subtropical jet in the form of meridionally trapped edge waves (Hoskins and Ambrizzi 1993).

Acknowledgments. This research was supported by the National Science Foundation through Grant No. ATM-9416701.

REFERENCES

Blackmon, M. L., J. M. Wallace, N.-C. Lau, and S. L. Mullen, 1977: An observational study of the Northern Hemisphere. *J. Atmos. Sci.,* **34,** 1040–1053.

Branstator, G., 1995: Organization of storm track anomalies by recurring low-frequency circulation anomalies. *J. Atmos. Sci.,* **52,** 207–226.

Dole, R. M., 1993: Deformation in planetary scale flows. Preprints, *Ninth Conf. on Atmospheric and Oceanic Waves and Stability,* San Antonio, TX, Amer. Meteor. Soc., 1–4.

Frederiksen, J. S., 1983a: Disturbances and eddy fluxes in Northern Hemisphere flows: Instability of three-dimensional January and July flows. *J. Atmos. Sci.,* **40,** 836–855.

——, 1983b: A unified three-dimensional instability theory of the onset of blocking and cyclogenesis. Part II: Teleconnection patterns. *J. Atmos. Sci.,* **40,** 2593–2609.

Hoskins, B. J., and P. J. Valdes, 1990: On the existence of storm-tracks. *J. Atmos. Sci.,* **47,** 1854–1864.

——, and T. Ambrizzi, 1993: Rossby wave propagation on a realistic longitudinally varying flow. *J. Atmos. Sci.,* **50,** 1661–1671.

Lee, S., 1995a: Localized storm tracks in the absence of local instability. *J. Atmos. Sci.,* **52,** 977–989.

——, 1995b: Linear modes and storm tracks in a two-level primitive equation model. *J. Atmos. Sci.,* **52,** 1841–1862.

——, and J. L. Anderson, 1996: A simulation of atmospheric storm tracks with a forced barotropic model. *J. Atmos. Sci.,* **53,** 2113–2128.

Lin, S. J., and R. T. Pierrehumbert, 1993: Is the midlatitude zonal flow absolutely unstable? *J. Atmos. Sci.,* **50,** 505–517.

Pierrehumbert, R. T., 1984: Local and global baroclinic instability of zonally varying flow. *J. Atmos. Sci.,* **41,** 2141–2162.

Simmons, A. J., J. M. Wallace, and G. W. Branstator, 1983: Barotropic wave propagation and instability, and atmospheric teleconnection patterns. *J. Atmos. Sci.,* **40,** 1363–1392.

Swanson, K. L., P. J. Kushner, and I. M. Held, 1997: Dynamics of barotropic storm tracks. *J. Atmos. Sci.,* **54,** 791–810.

Wallace, J. M., and N. C. Lau, 1985: On the role of barotropic energy conversions in the general circulation. *Adv. Geophys.,* **28A,** 33–74.

Whitaker, J. S., and R. M. Dole, 1995: Organization of storm tracks in zonally varying flows. *J. Atmos. Sci.,* **52,** 1178–1191.